Received 25 November 2024
Revised 27 November 2024
Accepted 27 November 2024

Cooperative maximum adhesion tracking control for multi-motor electric locomotives

Leiting Zhao and Yongxiang Wang
AC Transmission Department,
China Academy of Railway Sciences Corporation Limited, Beijing, China
Kan Liu
Locomotive and Car Research Institute,
China Academy of Railway Sciences Corporation Limited, Beijing, China
Liran Li
AC Transmission Department,
China Academy of Railway Sciences Corporation Limited, Beijing, China, and
Jingyuan Zhan and Qingliang Liu
School of Information Science and Technology, Beijing University of Technology, Beijing, China

Abstract

Purpose – This study aims to propose a cooperative adhesion control method for trains with multiple motors electric locomotives. The method is intended to optimize the output torque of each motor, maximize the utilization of train adhesion within the total torque command, reduce the train skidding/sliding phenomenon and achieve optimal adhesion utilization for each axle, thus realizing the optimal allocation of the multi-motor electric locomotives.

Design/methodology/approach – In this study, a model predictive control (MPC)-based cooperative maximum adhesion tracking control method for multi-motor electric locomotives is presented. Firstly, train traction system with multiple motors is constructed in accordance with Newton's second law. These equations include the train dynamics equations, the axle dynamics equations, and the wheel-rail adhesion coefficient equations. Then, a new MPC-based multi-axle adhesion co-optimization method is put forward. This method calculates the optimal output torque through real-time iteration based on the known reference slip speed to achieve multi-axle co-optimization under different circumstances.

Findings – This paper presents a MPC system designed for the cooperative control of multi-axle adhesion. The results indicate that the proposed control system is able to optimize the adhesion of multiple axles under numerous different conditions and achieve the optimal power distribution based on the reduction of train skidding/sliding.

Originality/value – This study presents a novel cooperative adhesion tracking control scheme. It is designed for multi-motor electric locomotives, which has rarely been studied before. And simulations are carried out in different conditions, including variable surfaces and motor failing.

Keywords Cooperative control, Adhesion control, Model predictive control, Slip prevent

Paper type Research paper

1. Introduction

Nowadays, the requirements for high adhesion force between wheels and rails are increasing, because most trains need high-speed, great acceleration and braking capacity. However, the

This research was supported by Scientific Research Projects of China Association of Metros (CAMET-KY-2022039) and State Key Laboratory of Traction and Control System of EMU and Locomotive (2023YJ386).

Railway Sciences
Vol. 4 No. 1, 2025
pp. 22-36
Emerald Publishing Limited
e-ISSN: 2755-0915
p-ISSN: 2755-0907
DOI 10.1108/RS-11-2024-0049

adhesion force between wheels and rails is not only affected by the motor output torque, but also related to the adhesion coefficient between the wheels and rails. In actual operation, the adhesion coefficient changes continuously due to dryness, rain, snow, icing and even oil and leaves, etc. Once the traction/braking torque provided by the traction motor is too large when the current adhesion state is relatively poor, the train will idle and skid, which will lead to damage to the tread surface, aggravate the abrasion of the wheels and rails. In extreme cases, it may even cause derailment and collision, resulting in traffic accidents and affecting the safety of train operation. Therefore, it is necessary to study the adhesion control method in order to maximize the adhesion force and prevent idling and skidding (Spiryagin, Lee, & Yoo, 2008).

There are number of research studies on adhesion between wheels and rails. In Kawamura *et al.* (2002), the authors suggest using the adhesion derivative as a control strategy signal. The slip speed command is corrected according to the slope of the adhesion curve. Some researchers have employed vector control and disturbance observer techniques to achieve precise regulation of the driving wheel torque (Kadowaki *et al.*, 2007). This approach has been instrumental in enhancing train adhesion properties and mitigating issues such as idling and slippage. In reference Cai, Li, and Song (2015) introduced an adaptive anti-skid adhesion control scheme. This scheme ensures control precision by dynamically updating observer parameters in response to the control error feedback from the closed-loop system. The article by Yao, Zhao, and Li (2024) enhances the tracking control of high-speed trains under complex adhesive dynamics by dynamically adjusting the control strategy and optimizing the train's traction force using the perturbation observer technique. This approach significantly improves the operational performance and safety of the train. Despite these advancements, traditional observer-based anti-slip and re-adhesion control methods fall short in optimizing the use of adhesion force and may not be fully compatible with the demands of modern train operations.

Research has shown that adhesion coefficient is a non-linear function slip (Ishikawa & Kawamura, 1997). Due to the unpredictable nature of wheel-rail contact conditions, which complicates the estimation of the adhesion coefficient, identifying the slip velocity that corresponds to maximum adhesion is inherently challenging (Abouzeid *et al.*, 2024). In reference (Sadr, Khaburi, & Rodriguez, 2016), a perturbation and observation (P&O) method, analogous to those employed in photovoltaic systems, was adapted to obtain the best operation point holding the maximum adhesion coefficient. This slip controller incrementally raises the commanded slip velocity while monitoring and logging the tractive force. Should the maximum point be exceeded, the slip velocity command is adjusted downward to return the operating point to a stable region. In reference (Wen, Huang, & Zhang, 2019), the authors proposed an anti-slip re-adhesion control system based on model predictive control (MPC). The system employs a second-order sliding mode observer to predict the adhesion coefficient, thereby determining the optimal slip speed. Subsequently, the distributed MPC controller ensures the train operates at the optimal adhesion point by tracking this optimal slip speed. The system's performance is rigorously validated through simulations and hardware-in-the-loop (HIL) testing. In the reference (Moaveni, Fathabadi, & Molavi, 2020), the authors introduced a supervisory predictive control system aimed at maximizing the starting acceleration and tracking the desired speed profile. The control strategy outlined in the article employs MPC to manage the longitudinal velocity of the train, thereby ensuring adherence to the desired speed profile and preventing wheel slip. Additionally, a fuzzy supervisory system is proposed to dynamically adjust the weighting parameters within the MPC's objective function, which is crucial for optimizing the starting acceleration. The authors in Abouzeid *et al.* (2024) explored advanced control strategies for maximizing wheel-rail adhesion and tracking desired speed profiles in railway traction drives. It proposed new methods that integrate fuzzy logic control and particle swarm optimization to overcome the limitations of existing adhesion tracking techniques. Through simulation and experimental validation, these new strategies demonstrate significant advantages in enhancing traction performance and reducing energy consumption. In reference Zirek and Onat (2020) proposed a swarm intelligence-based adhesion search method aimed at identifying the maximum adhesion coefficient. Lastly, in reference the

authors Zirek, Voltr, Lata, and Novák (2018) presented an adaptive sliding mode controller designed to stabilize vehicle slip and enhance traction performance. While these methods demonstrate promising adhesion performance, they face limitations such as the requirements of accurate measurement of the adhesion force and issues related to implementation complexity and high computational demands.

Despite the significant progress made in the field, there is a notable gap in the literature regarding the co-optimization of multiple axles. In actual train operations, the adhesion conditions can vary considerably between different wheel pairs, and it is essential to consider the co-optimization of multiple axles, particularly when they face diverse adhesion scenarios. Furthermore, there is a constraint on the output torque of the electric motor during train operation, which must be taken into account when designing and implementing control strategies for the train's propulsion system. Additionally, prolonged operation can lead to issues such as electric motor overheating and other suboptimal conditions, which should also be considered in the design of control systems to ensure reliable and efficient train operation.

Therefore, this paper proposes a multi-axle adhesion cooperative control system based on MPC. Firstly, the train traction system with multiple motors is established, including the vehicle dynamic, simplified axle dynamic model and the adhesion coefficient calculation model. Secondly, MPC-based cooperative controller for maximum adhesion tracking is designed. The MPC controller achieves adhesion cooperative control across multiple axles by dynamically adjusting the output torque of each pair wheel. Finally, simulation and analysis are performed under different conditions, including four cases.

2. Modelling of train traction system with multiple motors

The section introduces a multi-agent dynamic model for train traction system with multiple motors that have been utilized in the research. This comprehensive model encompasses several critical components:

(1) Vehicle dynamic model: This part of the model deals with the dynamics of a train that consists of multiple motors. It takes into account how these units interact and contribute to the overall motion of the train.

(2) Axle dynamics: This component focuses on the dynamics of the axles. This includes the forces and torques acting on the axles and their effect on the train's motion.

(3) Wheel-rail adhesion coefficient calculation models: This model calculates the adhesion coefficient between the wheels and the rails, which is a key factor in determining the tractive effort and braking performance of the train. The adhesion coefficient is influenced by various factors, including the condition of the wheel and rail surfaces, the presence of contaminants and environmental conditions.

2.1 Vehicle dynamic model

According to Newton's second law, conduct force analysis on the dynamic model of an n-axle train. For the entire vehicle, the train dynamics equation is as follows:

$$M\frac{dv_t}{dt} = \sum_{i=1}^{n} F_s^i - F_d \tag{1}$$

$$F_s^i = \mu^i\left(v_s^i\right)W^i g, i = 1, \ldots, n \tag{2}$$

$$F_d = \alpha + \beta v_t + \gamma v_t^2 \tag{3}$$

where v_t is the running speed of the train; M denotes the total mass of the train; F_s^i is the adhesion force between the wheels and the rails of the ith axle; F_d is the basic resistance of the train running, expressed specifically as a function about v_t, as shown in Eq. (3), where α, β, γ are coefficients related to the calculation of the basic resistance; μ^i is the adhesion coefficient of the ith axle; v_s^i is the sliding speed of the ith axle; W^i is the axle weight of the ith axle, $\sum_{i=1}^{n} W^i = M$. Under normal conditions, the axle weight of each axle is equally distributed, so $W^i = \frac{M}{n}, i = 1, \ldots, n$. However, in the presence of gradients, line unevenness and changes in hook height, the axle weight distribution will change. To account for this, an axle weight transfer influence coefficient can be introduced to adjust the axle weights to better reflect the actual operational conditions of the train.

2.2 Simplified axle dynamic model

In this paper, a simplified axle dynamics model is employed, as depicted in Figure 1. The rotational dynamics of the ith axle motor can be described by the following equation:

$$J_m^i \frac{dw_m^i}{dt} = T_m^i - T_L^i \tag{4}$$

where w_m^i is the output angular velocity of the ith axle motor, T_m^i is the output torque of the ith axle motor, J_m^i is the moment of inertia of the ith axle motor, and T_L^i is the load torque due to the adhesive force equivalent at the ith axle motor end.

The rotational dynamics of the ith axle are given by:

$$J_d^i \frac{dw_d^i}{dt} = T^i - F_s^i r \tag{5}$$

$$T^i = R_g T_L^i \tag{6}$$

$$R_g = \frac{w_m^i}{w_d^i} \tag{7}$$

where w_d^i is the angular velocity of the ith pair of axles, R_g is the vehicle gear ratio, J_d^i is the moment of inertia of the ith axle, and r is the radius of the wheel.

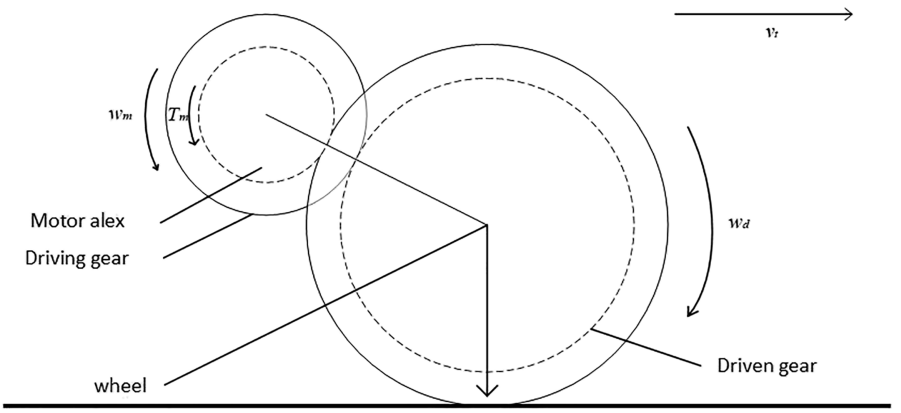

Source(s): Authors' own work

Figure 1. Simplified axle dynamic model

From equations (4) to (7), we derive the following equation:

$$J_{eq}^{i}\frac{dw_{m}^{i}}{dt}=T_{m}^{i}-\frac{r}{R_{g}}\mu^{i}\left(v_{s}^{i}\right)W^{i}g \tag{8}$$

where J_{eq}^{i} is the equivalent rotational inertia at the motor end of the ith axle. It can be calculated using the following equation:

$$J_{eq}^{i}=J_{m}^{i}+\frac{J_{d}^{i}}{R_{g}^{2}} \tag{9}$$

2.3 Adhesion coefficient calculation model

The coefficient of adhesion serves as an indicator of good wheel-rail contact. When a train initiates movement, the slip speed increases, which in turn causes the coefficient of adhesion to rise. However, after reaching a certain peak, the coefficient of adhesion begins to decrease as the slip speed continues to increase. Given that the coefficient of adhesion at any given moment is unpredictable and cannot be directly measured, Japanese scientists have analyzed extensive operational data from their railways to identify a general pattern. Based on this analysis, they have proposed an empirical formula that describes the curve of adhesion characteristics and the coefficient of adhesion (Ishikawa & Kawamura, 1997).

The expression of the adhesion characteristic curve is as follows:

$$\mu^{i}\left(v_{s}^{i}\right)=ce^{-av_{s}^{i}}-de^{-bv_{s}^{i}} \tag{10}$$

where the slip speed v_{s}^{i} is the difference between the peripheral wheel speed v_{w}^{i} and the train speed v_{t}:

$$v_{s}^{i}=v_{w}^{i}-v_{t} \tag{11}$$

a, b, c and d are related to the rail surface conditions. The values of the parameters under the two rail surfaces are shown in Table 1, and the values of the parameters of the empirical formulae vary under different rail surfaces.

The following figure illustrates the varying road surface conditions for underground vehicles in relation to the wheel-rail adhesion characteristics. In Figure 2, the vertical axis represents the adhesion coefficient, while the horizontal axis represents the slip speed.

As depicted in Figure 2, the adhesion characteristic curves under various road conditions exhibit distinct differences. The variation in road conditions is primarily influenced by factors such as climate, environment and human-induced pollution. For instance, dry and clean wheel treads and rail surfaces are associated with high adhesion coefficients. In contrast, during weather conditions like rain, snow, fog and frost, when the road surface is wet, the adhesion coefficient is significantly lower. The presence of oil pollution on the road surface further diminishes the adhesion coefficient (Lu, Song, & Cai, 2014; Pichlik & Zdenek, 2018).

Table 1. Parameter values of empirical equations for different surfaces

Surface	a	B	c	D
Dry	0.54	1.2	1.0	1.0
Wet	0.19	0.54	0.4	0.4

Source(s): Table courtesy of Li (2023)

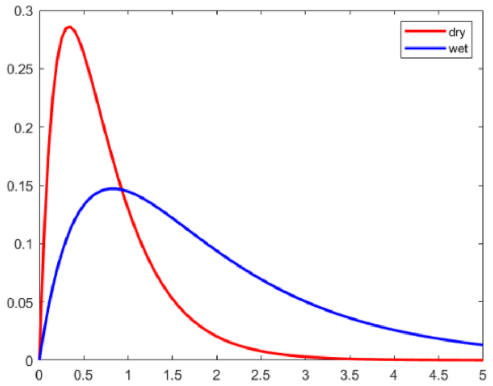

Source(s): Authors' own work

Figure 2. Wheel-rail adhesion curves at different surfaces

Despite the differences in characteristic curves, each has a corresponding maximum value for the coefficient of adhesion, denoted as μ_{max}, which is associated with a specific slip speed, v_{spot}. This pair, $(v_{\text{spot}}, \mu_{\max})$, represents the peak point of adhesion under the current road conditions. When the slip speed is less than v_{spot}, within the stable region, the adhesion coefficient increases with the slip speed, approximately in a linear fashion. Beyond v_{spot}, as the slip speed increases, the system enters an unstable region where the adhesion coefficient decreases rapidly with the increase in slip speed.

2.4 Multi-agent model of train traction system with multiple motors

The multi-agent model of the train traction system with multiple motors can be obtained based on Eqs. (1)-(3) and Eqs. (8)-(11):

$$\begin{cases} \dfrac{dv_s^i}{dt} = \dfrac{r}{R_g J_{eq}^i} \cdot T_m^i - \dfrac{r^2 W^i g}{R_g{}^2 J_{eq}^i} \mu^i\left(v_s^i\right) - \dfrac{g}{M} \displaystyle\sum_{i=1}^{n} W^i \mu^i\left(v_s^i\right) + \left(\alpha + \beta v_t + \gamma v_t^2\right) \Big/ M, \\ \qquad\qquad i = 1, \ldots, n \\ \dfrac{dv_t}{dt} = \dfrac{g}{M} \displaystyle\sum_{i=1}^{n} W^i \mu^i\left(v_s^i\right) - \left(\alpha + \beta v_t + \gamma v_t^2\right) \Big/ M \end{cases} \tag{12}$$

Assume that the state variable is $x = [v_s^1, v_s^2, \ldots, v_s^n, v_t]^T$, the control input variable is $u = [T_m^1, T_m^2, \ldots, T_m^n]^T$ and the output variable is $y = [v_s^1, v_s^2, \ldots, v_s^n]^T$. The state space equation of the system can be constructed according to Eq. (12), and it is expressed as follows:

$$\dot{x} = f(x, u) \tag{13}$$

$$y = Cx \tag{14}$$

where $C = [I_n \quad 0]$. It shows that the system is a dynamically coupled nonlinear multi-agent system with n inputs and n outputs.

We propose to use the MPC method for the control inputs $u = [T_m^1, T_m^2, ..., T_m^n]^T$ for optimization, and in order to facilitate the design of the controller, the state space equation (10) is first discretized to obtain the offline model as:

$$x(k+1) = x(k) + Tf(x(k), u(k)) = F(x(k), u(k)) \tag{15}$$

where T is the sampling time.

3. Cooperative controller for maximum adhesion tracking

In this section, we utilize a MPC approach to co-optimize the output torque of each motor within the multi-motor locomotive system, which is predicated on the previously discussed multi-agent model. The primary control objective is to accurately track the reference slip speed trajectory.

Given the total motor torque command value T_m^* and the reference slip velocity trajectory $v_s^{i,ref}(k)$ for any i-axle ($i = 1, ..., n$), the multi-agent adhesion co-optimization objectives are as follows:

(1) The sum of the output torques of multiple motors tracks T_m^*.

(2) The slip speed of any i-axle tracks its reference value $v_s^{i,ref}$.

(3) Prevent the wheel slipping.

(4) Optimize the distribution of the power.

These objectives aim to meet the commanded torque value while preventing the train from idling or skidding. Additionally, they seek to maximize the utilization of the available tractive force under the given road conditions. This is achieved by optimizing the adhesion for each individual wheel-pair, thereby leading to an optimal allocation of traction power among the multi-axle traction power units. The goal is to achieve an optimal distribution of the multiple power, ensuring both safety and efficiency in the train's operation.

3.1 Objective function

Let $v_s^{ref} = [v_s^{1,ref}, v_s^{2,ref}, ..., v_s^{n,ref}]^T$, to achieve the tracking of the reference slip speed $v_s^{i,ref}$ for any i-axle, the objective function of the predictive controller at time step k is formulated as follows:

$$J(k) = \sum_{j=1}^{N_p} \left\| y(k+j|k) - v_s^{ref}(k+j) \right\|_Q^2 + \sum_{j=0}^{N_c-1} \left\| u(k+j|k) \right\|_R^2 \tag{16}$$

where Q and R are weight matrices, we require Q to be a semi-positive definite matrix and R to be a positive definite matrix. N_p is the prediction horizon and N_c is the control horizon. The first term in Eq. (13) reflects the ability of the system to track the reference slip speed and the second term represents the energy consumption of the system.

3.2 Constraint

The constraint design must adhere to the following requirements: due to the limitations of the traction motor within the traction system, the torque output from the predictive control must not surpass the effective torque command value T_{limit} provided by the Traction Control Unit (TCU). To achieve the sum of the multi-motor output torque tracking T_m^*, the equation $T_m^1 + T_m^2 + ... + T_m^n = T_m^*$ must hold true. Additionally, the reference slip speed must be ensured not to exceed the maximum sticking point, and a relaxation factor is included to ensure

the operational safety of the traction system. Based on these constraint requirements, the controller's constraint design can be formulated as follows:

$$\begin{cases} 0 \le T_m^i \le T_{limit} \\ T_m^1 + T_m^2 + \ldots + T_m^n = T_m^*, \ i = 1, \ldots, n \\ v_s^{i,ref} - \varepsilon \le v_s^i \le v_s^{i,ref} + \varepsilon \end{cases} \tag{17}$$

3.3 Optimal control problem

Establish the MPC optimization problem at moment k as follows:

$$\min_{\{u(k+j|k)\}_{j=0}^{N_c-1}} J(k) \tag{18}$$

s.t. (15), (17)

At moment k, by solving the above nonlinear optimization problem with constraints, the optimal output torque of all motors $T_m^{1*}, T_m^{2*}, ..., T_m^{n*}$. The solution of the above optimization problem is repeated with $x(k+1)$ as the initial value at the moment $k+1$.

3.4 Model predictive control algorithm

The MPC algorithm is shown as follows:

(1) Initialization

At time t = 0, assume that the train starts from a standstill. Initialize the assumed values as follows:

$$\begin{cases} u(k|0) = u(0) \\ y(k|0) = y(0) \end{cases}, k = 0, 1, \cdots, N_P - 1, \tag{19}$$

where the predicted output can be derived from Eq. (13) and Eq. (14).

(2) Iteration

When t > 0:

- MPC controller solves the optimal control problem $J(k)$ and obtains the optimal predictive control input $u^*(k|t)$,
- Using the obtained optimal control input $u_i^*(k|t)$ to find the optimal state $x^*(k|t)$ within the prediction range,

$$x^*(0|t) = x(0|t) \tag{20}$$

$$x^*(k+1|t) = f(x^*(k|t), u^*(k|t)) \tag{21}$$

- Extract the first term of the optimal predictive control input $u_i^*(k|t)$ as the actual system control input,

$$u(t) = u^*(0|t) \tag{22}$$

- Calculate the actual state and output using the train dynamics equations,
- $t = t + 1$, and repeat the above steps until the end of the loop.

4. Simulation and analysis

In this section, we construct a multi-motor locomotives dynamics system model within the MATLAB simulation environment to demonstrate the efficacy of the MPC systems proposed herein. The simulations are executed utilizing the actual parameters of the ER24PC locomotive, as detailed in Table 2. This locomotive was manufactured by MAPNA Locomotive Engineering and Manufacturing Company in collaboration with Siemens, specifically the Iran-Safir locomotive (Moaveni *et al.*, 2020). Throughout the simulations, the prediction horizon is set to $N_P = 10$ and the control horizon to $N_C = 5$. It is evident that reducing the prediction horizon can alleviate computational demands but may adversely affect the closed-loop system responses. The simulation parameters are presented in Table 2.

The reference slip speed of the train is known and the train motor torque command limit is used as the system constraint. The total simulation time is 30s, and two different track surface conditions are set: dry and wet track surface. The simulations have been done in four cases, for different conditions.

4.1 Case1: all axle on dry-wet-dry surface

In this case, it is assumed that the train is traveling alternately in dry and wet track surface, and all motor of the train are working normally. Firstly, the train starts from the dry wheel-rail surface and enters the wet wheel-rail surface after 10 seconds. At 20s, the train re-enters the dry wheel-rail surface. The reference slip speed ${v_s}^{ref}$ of the train and the actual slip speed v_s^i of each axle in case 1 are shown in Figure 3(a), and the error between the reference slip speed ${v_s}^{ref}$ and the actual slip speed v_s^i of each axle is shown in Figure 3(b). The traction torque output T_m^i of each axle is shown in Figure 3(c), and the adhesion coefficient μ^i of each axle of the train is shown in Figure 3(d).

After the train starts on the dry wheel-rail surface, it runs on the dry wheel-rail surface from 0-10s. As shown in Figure 3(a) and (b), the slip speed of each axle of the train tracks the reference slip speed, and the error decreases rapidly. From Figure 3(c) and (d), it can be seen that the adhesion coefficient stays around 0.27 after a very short period of time, and the output torque of each motor rises rapidly from 1500N·m to around 4200N·m. At 10s, the train enters the wet wheel-rail surface, the reference slip speed changes at the same time. And the actual slip speed changes greatly with switching track surfaces, so that the tracking error appears an extremely large value. The motor output torque decreases rapidly to inhibit wheel idling, the motor output torque reduces to 2200N·m and the adhesion coefficient reduces to about 0.14. After 20s, the train returns to the dry wheel-rail surface, the actual slip speed decreases rapidly,

Table 2. simulation parameters

Parameter	Value
M	14,167 kg
g	9.8 m/s^2
r	0.5 m
R_g	4.13
J_{eq}^i	146.7 $kg \cdot m^2$
Np	10
Nc	5
T	0.1 s

Source(s): Table courtesy of Moaveni *et al.* (2020)

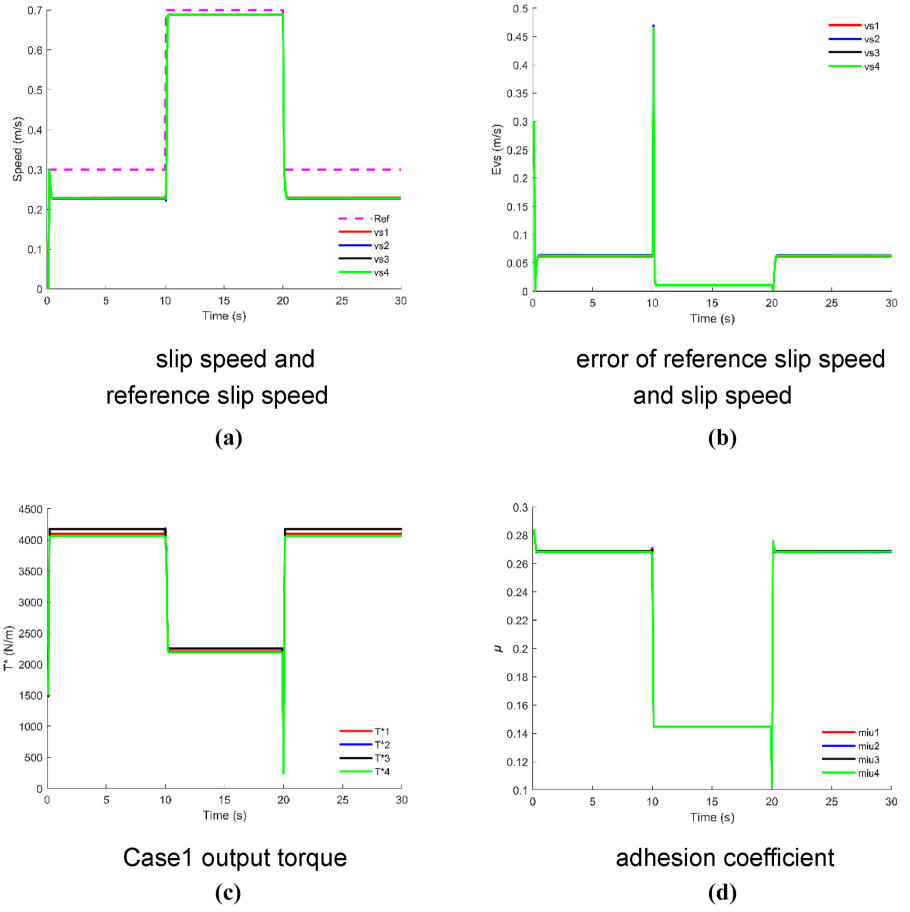

Source(s): Authors' own work

Figure 3. Case1: dry-wet-dry surface

the adhesion coefficient and output torque rise to the values in the period of 0-10s. The output torque of each axle does not exceed the system constraint of 5000 $N \cdot m$ and the total output torque does not exceed 16,500 $N \cdot m$ during the whole simulation process. It should be noted that the output torque and slip speed fluctuate during the track surface switching, which causes the wheels to idle, but the control system recovers the adhesion in a short time to achieve the tracking of the desired slip speed.

Tips: constrained by the total torque, the torque output cannot simultaneously satisfy the minimum tracking error when the wheel-rail surface is dry. When the required torque decreases in the wet surface, the controller is able to calculate the torque output that tracks better within the constraints.

4.2 Case 2: only one axle on dry-wet-dry surface

In this case, it is assumed that only the wheel-rail surface of the axle 4 changes. It implies that axles 1 to 3 always move on the dry rail surface. Axle 4 initially travels on the dry rail surface. At the 10th second, the wheel-rail surface of 4th axle changes to wet. Then, at 20 seconds, it

returns to the dry wheel-rail surface. The reference slip speed v_s^{ref} and the actual slip speed v_s^i of each axle in case 2 are shown in Figure 4(a), and the error between the reference slip speed v_s^{ref} and the actual slip speed v_s^i is shown in Figure 4(b). The adhesion coefficient μ^i of each axle is shown in Figure 4(c) and the traction torque output T_m^i of each axle is shown in Figure 4(d).

The initial condition is unchanged. When axle 4 enters the wet wheel-rail surface after 10 seconds, due to the change in the wheel-rail surface, axle 4 should reduce torque output and increase slip speed in order to increase the adhesion coefficient. As the torque output of axle 4 decreases, the torque output of axles 1 to 3 can increase to achieve better acceleration and reduce the impact caused by the change of the wheel-rail surface on 4-axle. At 20 seconds, the surface of axle 4 recovers and the system returns to the dry condition.

4.3 Case 3: two axles on dry-wet-dry surface

In this case, the wheel-rail of axles 3 and 4 change while axles 1 and 2 are unchanged. The details are as follows: at 0-10s, axles 1–4 are all running on the dry wheel-rail surface, and axles 1 and 2 are unchanged with the axles 3 and 4 changing to the wet wheel-rail surface at 10-

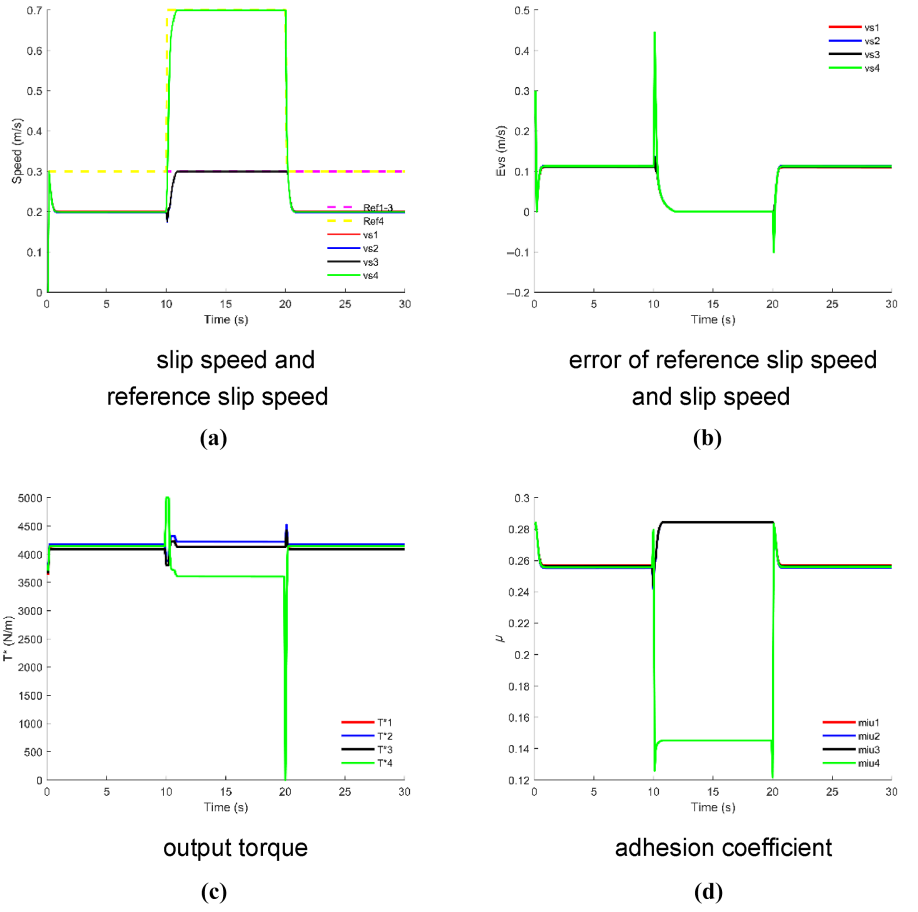

Source(s): Authors' own work

Figure 4. Case 2: only one axle on dry-wet-dry surface

20s. After 20s, axles 3 and 4 return to the dry wheel-rail surface. The simulation results are shown in Figure 5.

The train still starts on the dry wheel-rail surface. As shown in Figure 5, after 10s, the torque of the axle 3 and axle 4 drop rapidly. When one axle enters the wet condition (Case2), the overall speed of the train is less affected. However, it will have a significant impact on the train speed that the two axles wheel-rail surface change at the same time. Even if the controller quickly adjusts the torque distribution, the train's speed growth visibly decreases.

4.4 Case 4: motor failing on dry-wet-dry surface

The simulation scenario presented pertains to a situation where the motor of axle 4 is malfunctioning. Specifically, during transitions on the rail surface or prolonged operation, the 4-axle motor may fail to achieve the desired torque output due to factors such as overheating or unforeseen conditions. Upon detecting this, the system reallocates torque to mitigate the impact of the motor's suboptimal performance on the train's operational speed and to optimize torque utilization. The detailed steps are as follows:

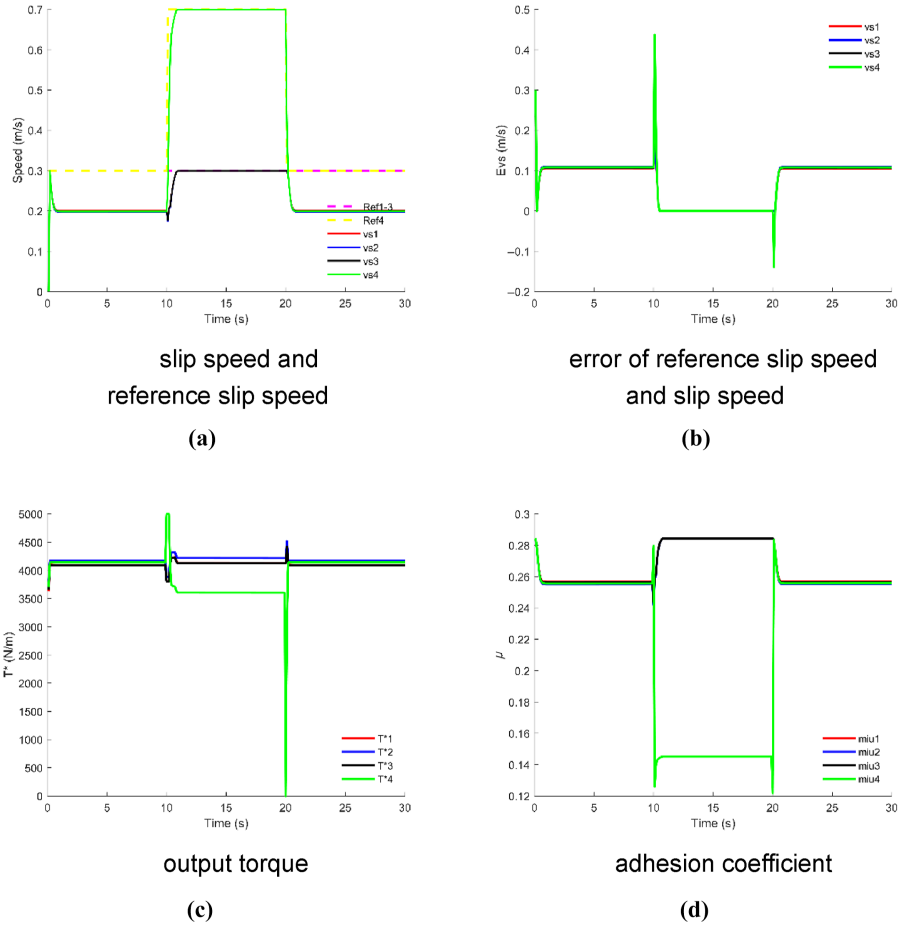

Source(s): Authors' own work

Figure 5. Case 3: two axles on dry-wet-dry surface

(1) The train commences its journey on the dry wheel-rail surface at time zero. From 0 to 10 seconds, all train motors function normally.

(2) At 10 seconds, as the wheel-rail surface transitions to wet, the axle 4 motor fails, impeding its ability to achieve the desired output torque.

(3) At 20 seconds, the wheel-rail surface reverts to dry, yet the axle 4 motor remains in a failed state.

(4) By 25 seconds, the axle 4 motor resumes normal operation.

The results of this simulation are depicted in Figure 6.

As depicted in Figure 6, the failure of the motor results in a diminished tracking efficacy for axle 4. This degradation is a direct consequence of the motor's malfunction. Despite the controller's attempt to augment the output torque, the maximum adhesion coefficient on the wet wheel-rail interface poses a constraint on the available adhesion. Consequently, between 10 to 20 seconds, there is a negligible variation in the desired output torque commanded by the controller for axles 1–3 compared to axle 4. Upon transitioning to a dry rail surface, the

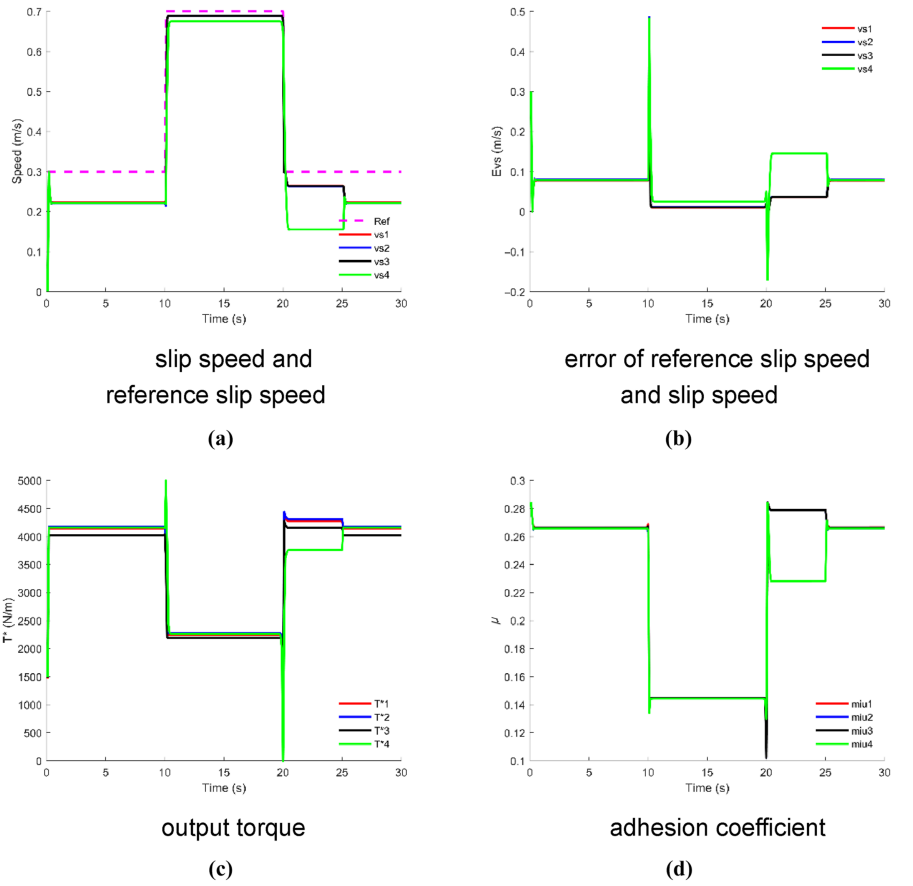

Source(s): Authors' own work

Figure 6. Case 4: motor failing on dry-wet-dry surface

adhesion limitation is predominantly governed by the motor's capacity. Hence, the system increases the torque allocation to axles 1 to 3 while reducing the torque assigned to axle 4 to mitigate the impact of the motor failure on axle 4. Once the motors are restored, the system is capable of reallocating torque in a rational manner, ensuring an equitable distribution of torque among the various motors.

5. Conclusion

This paper presents a MPC system designed for cooperative maximum adhesion tracking control system for multi-motor electric locomotives. The system aims to track a reference slip speed, prevent train idling and optimize the distribution of multi-axle adhesion forces, all while complying with pertinent torque constraints. The research commences with an overview of the multi-motor locomotive model, which integrates train dynamics, axle dynamics and formulae for determining adhesion coefficients. The MPC serves as the system controller, responsible for adjusting the power distribution across each axle. The efficacy of the proposed control strategy is substantiated through simulations executed in the MATLAB environment, encompassing four distinct scenarios.

Looking ahead, it is recommended that the performance of the control system outlined in this paper be further appraised through semi-physical simulations and by implementing hardware-in-the-loop experiments during actual train operations. It will provide a more comprehensive assessment of the system's capabilities and reliability in real-running scenarios.

References

Abouzeid, A. F., Guerrero, J. M., Lejarza-Lasuen, L., Muniategui-Aspiazu, I., Endemaño-Isasi, A., & Briz, F. (2024). Advanced maximum adhesion tracking strategies in railway traction drives. *IEEE Transactions on Transportation Electrification*, *10*(2), 3645–3660. doi: 10.1109/TTE.2023.3312621.

Cai, W. -C., Li, D. -Y., & Song, Y. -D. (2015). A novel approach for active adhesion control of high-speed trains under antiskid constraints. *IEEE Transactions on Intelligent Transportation Systems*, *16*(6), 3213–3222. doi: 10.1109/TITS.2015.2440654.

Ishikawa, Y., & Kawamura, A. (1997). Maximum adhesive force control in super high speed train. *Proceedings of Power Conversion Conference - PCC '97*, *2*(2), 951–954. doi: 10.1109/PCCON.1997.638382.

Kadowaki, S., Ohishi, K., Hata, T., Iida, N., Takagi, M., Sano, T., & Yasukawa, S. (2007). Antislip readhesion control based on speed-sensorless vector control and disturbance observer for electric commuter train—series 205-5000 of the East Japan railway Company. *IEEE Transactions on Industrial Electronics*, *54*(4), 2001–2008. doi: 10.1109/TIE.2007.895135.

Kawamura, A., Furuya, T., Takeuchi, K., Takaoka, Y., Yoshimoto, K., & Cao, M. (2002). Maximum adhesion control for shinkansen using the tractive force tester. In *IEEE 2002 28th Annual Conference of the Industrial Electronics Society. IECON 02* (Vol. 1, pp. 567–572), 1 doi: 10.1109/IECON.2002.1187570.

Li, Z. (2023). *Research on locomotive adhesion ontrol method based on predictive control*. MA dissertation. Chengdu, China: Southwest Jiaotong University.

Lu, K., Song, Y., & Cai, W. (2014). Robust adaptive re-adhesion control for high speed trains. In *17th International IEEE Conference on Intelligent Transportation Systems (ITSC)* (pp. 1215–1220). doi: 10.1109/ITSC.2014.6957853.

Moaveni, B., Fathabadi, F. R., & Molavi, A. (2020). Supervisory predictive control for wheel slip prevention and tracking of desired speed profile in electric trains. *ISA Transactions*, *101*, 102–115. doi: 10.1016/j.isatra.2020.01.011.

Pichlik, P., & Zdenek, J. (2018). Locomotive wheel slip control method based on an unscented Kalman filter. *IEEE Transactions on Vehicular Technology*, *67*(7), 5730–5739.

Sadr, S., Khaburi, D. A., & Rodriguez, J. (2016). Predictive slip control for electrical trains. *IEEE Transactions on Industrial Electronics*, *63*(6), 3446–3457. doi: 10.1109/TIE.2016.2543180.

Spiryagin, M., Lee, K. S., & Yoo, H. H. (2008). Control system for maximum use of adhesive forces of a railway vehicle in a tractive mode. *Mechanical Systems and Signal Processing*, *22*(3), 709–720. doi: 10.1016/j.ymssp.2007.09.018.

Wen, X., Huang, J., & Zhang, S. (2019). Anti-slip Re-adhesion control strategy of electric locomotive based on distributed MPC. In *2019 IEEE 21st International Conference on High Performance Computing and Communications; IEEE 17th International Conference on Smart City; IEEE 5th International Conference on Data Science and Systems (HPCC/SmartCity/DSS)* (pp. 2708–2713). doi: 10.1109/HPCC/SmartCity/DSS.2019.00380.

Yao, X., Zhao, B., & Li, S. (2024). Disturbance observer-based tracking control of high-speed trains under adhesion dynamics. *IEEE Transactions on Automation Science and Engineering*, *21*(2), 1727–1739. doi: 10.1109/TASE.2023.3238811.

Zirek, A., & Onat, A. (2020). A novel anti-slip control approach for railway vehicles with traction based on adhesion estimation with swarm intelligence. *Railway Engineering Science*, *28*(4), 346–364. doi: 10.1007/s40534-020-00223-w.

Zirek, A., Voltr, P., Lata, M., & Novák, J. (2018). An adaptive sliding mode control to stabilize wheel slip and improve traction performance. *Proceedings of the Institution of Mechanical Engineers, Part F: Journal of Rail and Rapid Transit*, *232*(10), 2392–2405. doi: 10.1177/0954409718774139.

Corresponding author
Kan Liu can be contacted at: bjliukan@163.com